Supplement of The Cryosphere, 16, 1889–1901, 2022
https://doi.org/10.5194/tc-16-1889-2022-supplement

The Cryosphere Open Access EGU

Supplement of

High nitrate variability on an Alaskan permafrost hillslope dominated by alder shrubs

Rachael E. McCaully et al.

Correspondence to: Carli A. Arendt (carendt@ncsu.edu)

Sample Collection

In-situ parameters: In-situ parameters were measured for each water sample and included depth to frozen soil or bedrock, soil temperature, soil pore water pH, dissolved oxygen, and specific conductivity. A 1 m steel frost probe was used to measure the depth (cm) to frozen soil, roots, or bedrock at each location. Depths were averaged from three measurements per rhizon nest. Soil temperature was measured in tandem with soil depth measurements using an Orion thermometer. An Orion pH meter and YSI multi-parameter meter were used to collect *in situ* hydrochemistry parameters in unfiltered samples upon collection. Dissolved oxygen (DO) was measured in July 2017 and 2018 using a Hach Portable Optical DO Probe or YSI multi-parameter meter.

Analysis

Soil pore water concentrations: Samples were immediately filtered with a 1.5 μm pre-filter and a 0.45 μm filter and stored in HDPE Nalgene bottles for major cation and anion analysis. Anion samples were frozen and cation samples were preserved to a pH < 2 with nitric acid and frozen. Cations were measured using inductively coupled plasma optical emission spectrometry (ICP-OES) on a Perkin Elmer Optima 2100DV instrument (Perkin Elmer Inc., USA) using United States Environmental Protection Agency (EPA) method 200.7; precision is justified to 0.01 mg L^{-}. Anions were measured with ion chromatography on a Dionex ICS-2100 instrument (Thermo Fisher Scientific Inc., USA) utilizing EPA method 300 (Throckmorton *et al*., 2015); precision is justified to 0.01 mg L^{-1}. Ammonium (NH_4^+) concentrations were determined for a subset of samples (n = 92) with a modified Berthelot method with a limit of quantitation of 0.03 mg L^{-1} by UV-VIS spectroscopy using a Cary 100 Bio UV-Visible Spectrophotometer (Agilent Inc., USA).

Soil and leaf litter: Pebbles, roots, and leaf litter were removed from the tins upon collection to avoid any mass bias. Gravimetric soil moisture was measured where soil and tins were weighed, dried at 80° C for a minimum of 72 hours, and reweighed. Soil moisture was determined as the difference in mass between wet and dry soil. Thirteen soil samples and five leaf litter samples were analyzed for total N, $\delta^{15}N$ of soil organic nitrogen (SON) and C/N ratios using a Costech Elemental Analyzer coupled to a Thermo Delta V IRMS.

Isotopic Insights

Isotopic approach: Isotopic values are reported in delta (δ) notation as the deviation from an established standard in units per mil (‰) as the deviation from a standard of known composition, atmospheric N_2 for NO_3^- and VSMOW (Vienna Standard Mean Ocean Water) for water. Isotopic data for $\delta^{15}N$ and $\delta^{18}O$ of soil pore water and soil pore water NO_3^--N were measured using the methods outlined in Heikoop *et al.,* (2015); precision is justified to 0.1 ‰. A modified denitrifier method outlined by Sigman *et al.* (2001) and Casciotti *et al.* (2002) was used and analyses were made using a GV Isoprime isotope ratio mass spectrometer (IRMS) coupled to a TraceGas peripheral.

The production of NO_3^- through nitrification is a microbially mediated process that produces predictable isotopic compositions through kinetic fractionation (Kendall and McDonnell, 1998). Based on the assumption that microbial nitrification utilizes two oxygen (O) atoms from water (H_2O) and one O atom from the atmosphere (O_2), the expected range of $\delta^{18}O$ – NO_3^- derived from microbial nitrification (Kendall and McDonnell, 1998) was calculated using Eq. (S1):

$$\delta^{18}O - NO_3^- = \frac{2}{3}(\delta^{18}O - H_2O) + \frac{1}{3}(\delta^{18}O - O_2), \quad \text{(S1)}$$

where atmospheric $\delta^{18}O\text{-}O_2$ is +23.5 ‰ (Kendall and McDonnell, 1998). Isotopic data for $\delta^{18}O$ - H_20 was measured directly from soil pore water samples using a GV Instruments Multiflow peripheral instrument (Heikoop *et al.*, 2015). The concentration of dissolved organic nitrogen (DON) was calculated as the difference between total dissolved nitrogen (TDN-N) (measured using persulfate oxidation) and NO_3^--N (Eq. (S2), assuming negligible concentrations of other inorganic N species), and the range of δ^{15}N-DON was derived using Eq. (S3). $\delta^{15}N_{TDN}$ was measured from the sample aliquots that underwent persulfate oxidation for TDN, which converts all ammonium, DON, and nitrite to nitrate. Thus, the $\delta^{15}N_{TDN}$ is from δ^{15}N analyses of the TDN sample aliquot.

$$[DON] = [TDN] - [NO_3^-], \quad \text{(S2)}$$

$$\delta^{15}N_{DON} = \frac{(\delta^{15}N_{TDN} \times [TDN]) - (\delta^{15}N_{NO3} \times [NO_3^-])}{[\text{DON}]}, \quad \text{(S3)}$$

Isotopic results: A total of 62 soil pore water samples from locations within and downslope of alder shrubland had sufficient NO_3^- concentrations (> 0.5 mg L^{-1}) to measure δ^{15}N and δ^{18}O of NO_3^- across all four sampling campaigns (Fig. S2). Generally, $\delta^{15}N - NO_3^-$ at lowland locations downslope of the alder shrubland were more enriched than locations within alder shrubland, and high $\delta^{18}O - NO_3^-$ values correspond to high $\delta^{15}N - NO_3^-$ values at the downslope locations (Fig. S2). Because minimal fractionation takes place during N_2 fixation, NO_3^- produced by mineralization and nitrification of organic matter derived from fixation (alder leaf litter) should have $\delta^{15}N\text{-}NO_3^-$ in the range of -5.0 ‰ to 5.0 ‰ (Kendall and McDonnell, 1998). δ^{15}N of leaf litter N (n=10; 5 samples were originally collected but later each were subdivided to allow a replicate of each) collected from the shrubland along all five transects (along with δ^{15}N data from

Salmon et al., 2019; n=5) ranged from -2.8 ‰ to -0.9 ‰. $\delta^{15}N$ of total dissolved nitrogen (TDN) ranged from -11.3 ‰ to -0.9 ‰, and $\delta^{15}N$ of dissolved organic nitrogen (DON) ranged from -19.1 ‰ to -8.0 ‰. $\delta^{15}N$ of soil organic nitrogen (SON) ranged from 0.5 ‰ to 3.6 ‰ (n = 13). Atmospheric NO_3^- values of $\delta^{15}N$ range from ~ -15 ‰ to ~ +15 ‰ and $\delta^{18}O$ ranging from ~ +60 ‰ to ~ +94 ‰ (Granger and Wankel, 2016). A summary of $\delta^{18}O$ compositions is provided Table S7. T-tests were performed to identify significant differences between $\delta^{18}O$ during each campaign.

Isotopic discussion: On the KG Hillslope, isotopic signatures of NO_3^- from all but two collections fall within the expected range of $\delta^{18}O$ - NO_3^- of microbially derived NO_3^- (Fig. S2), further indicating that the soil pore water NO_3^- is a product of microbial mineralization and nitrification rather than atmospheric deposition (Schimel and Bennett, 2004). To determine the range of $\delta^{18}O$-NO_3^-derived from microbial nitrification, we used Eq. (S1). However, other studies suggest that $\delta^{18}O$-NO_3^- should more closely represent $\delta^{18}O$-H_2O (Boshers et al., 2019). We determined the range of $\delta^{18}O$-NO_3^- derived by microbial nitrification to encapsulate both possibilities, shown in Fig. S2. If the source of NO_3^- was by atmospheric deposition, values of $\delta^{15}N$ between ~ -15 ‰ and ~ +15 ‰ and $\delta^{18}O$ between ~ +60 ‰ and ~ +94 ‰ would be expected (Granger and Wankel, 2016).

In September 2017 and September 2018, some samples collected within the shrubland along the A1 and A4 transects had light $\delta^{15}N$-NO_3^- (< -8.0 ‰; Fig. S4). These values are likely representative of nitrification of DON derived from non-alder sources (Fig. S2). For example, measurements of leaf $\delta^{15}N$ from moss, lichen, and dwarf shrubs growing upslope from the alder

shrublands at the KG Hillslope range from -13.78 ‰ to -8.45 ‰ (Salmon et al., 2019). Nitrogen from these plant types may have been mobilized downslope from the alder shrubland, resulting in the depleted $\delta^{15}N$ found within our samples.

A precipitation event may be partially reflected in the isotopic composition of water samples collected in September 2017, which had an average $\delta^{18}O$ value of -15.6 ± 0.8 ‰; ~1 ‰ more enriched than water samples collected in July 2017, July 2018, and September 18 ($p<0.001$; Fig. S3 and Table S7). However, without the direct isotopic analyses of precipitation samples, these interpretations are based solely on the co-occurrence of precipitation events with observed chemical variability and are not quantitatively verified. Soil pore water in the upland area was heavier in $\delta^{18}O$ composition (-15.62 ± 0.86 ‰) than in the lowland area (-16.56 ± 0.48 ‰), though these ranges overlap (0.40 ‰; Fig. S5). The steep slopes in the upland area also promote prompt drainage of rainfall and active layer melt towards the lowlands, where the transition to a lower gradient, lack of evaporation, and limited vertical drainage result in increased residence times and increased storage capacity.

In a reducing environment, enrichment of $\delta^{15}N$ and $\delta^{18}O$ occurs during the process of microbial denitrification (Böttcher et al., 1990). In freshwater systems, this enrichment is typically expressed as a 1:1 ($\delta^{18}O$/ $\delta^{15}N$) relationship, though many systems have trajectories greater or less than 1 (Boshers et al., 2019). Deviations from a trajectory of 1 may be a result of nitrification and/or annamox (anaerobic ammonium oxidation) that produces NO_3^- concurrently during denitrification in anoxic conditions (Granger and Wankel, 2016). The locations downslope of alder shrublands follow a similar trend of enrichment in $\delta^{15}N$ and $\delta^{18}O$ with an

apparent regression slope of 0.84 (Fig. S2), suggesting denitrification occurring in the lowland areas.

Based on isotopic observations, soil pore water from the lowland active layer may have had a greater component of isotopically lighter and older spring rainfall/snowmelt and active layer ice melt, while the upland area reflected isotopically enriched, younger summer rainfall relative to our sampling campaigns (Kendall and McDonnell, 1998). Active layer ice in the less well-drained lowland areas would therefore also be expected to be lighter and to contribute more to the isotopic mass balance than in the upland area. Thus, the isotopic composition of water in upland soils likely reflects a larger summer rainfall component while lowland soils likely reflect isotopically lighter active layer ice melt (Throckmorton et al., 2015; Craig, 1961). These precipitation interpretations should be considered carefully as we were unable to directly measure the $\delta^{15}N$ and $\delta^{18}O$ of local precipitation due to logistical and sampling constraints. However, we apply logical inferences about likely influences of precipitation on observed chemical trends from our field location based on the known occurrence of rain events on specific sampling days and the corresponding shifts in site chemistry observed.

Coefficient of Variability

The coefficient of variability was calculated for Ca, Na, Cl^- and NO_3-N (Table S3) to directly compare the variability of each constituent across the landscape, where ratios closer to zero indicate less variation (Brown, 1998). Ca, Na, and Cl^- are all compounds that typically have

low variability within the environment. Consistently high ratios of NO_3-N (> 1.5) and low ratios of Ca, Cl^-, and Na (< 1.5) indicate additional (biological) processes acting on NO_3^- availability.

Supplemental Tables

Table S1: Ammonium concentrations measured in September 2017, July 2017, and September 2019. Values < 0.02 mg L^{-1} are not reported. Black horizontal lines separate sampling campaigns.

Date	*Chemical Parameter (mg L^{-1})*	*n*	*max*	*min*	*mean*	*std*
July-17	NH_4^+	1	0.08	0.08	-	-
Sept-17	NH_4^+	2	0.29	0.03	0.16	0.18
July-18	NH_4^+	13	0.08	0.02	0.04	0.02

Table S2: *In situ* chemical parameters measured during each sampling campaign. No measurements were collected in September 2018. Black horizontal lines separate sampling campaigns. No obvious spatial or temporal trends were observed within these parameters.

Date	*Chemical parameter*	*n*	*min*	*max*	*mean*	*std*
17-Jul	Dissolved Oxygen (mg L^{-1})	45	1.93	7.98	4.71	1.72
	pH	48	4.97	7.34	5.76	0.54
	Conductivity (µS cm^{-1})	-	-	-	-	-
17-Sep	Dissolved Oxygen (mg L^{-1})	3	3.86	7.04	4.97	1.79
	pH	20	4.74	6.42	5.47	0.44
	Conductivity (µS cm^{-1})	-	-	-	-	-
18-Jul	Dissolved Oxygen (mg L^{-1})	114	1.34	6.76	3.54	1.15
	pH	114	3.77	9.97	5.41	0.67
	Conductivity (µS cm^{-1})	114	0.02	0.16	0.07	0.04

Table S3: Coefficient of variability ratio for calcium, sodium, chloride, and nitrate-N on upland and lowland locations. July 2017 through September 2018. Black horizontal lines separate sampling campaigns.

Date	*Location*	*Ca*	*Na*	*Cl^-*	*NO_3-N*
All	Upland	0.69	0.43	1.40	1.89
	Lowland	0.88	0.27	1.24	2.08
Jul-17	Upland	0.41	0.29	1.22	2.02

	Lowland	0.77	0.35	1.18	1.17
	All Locations	0.90	0.34	1.35	3.29
Sep-17	Upland	0.46	0.14	0.55	1.45
	Lowland	0.38	0.14	0.67	2.11
	All Locations	0.46	0.33	0.93	2.03
Jul-18	Upland	0.51	0.27	0.43	1.06
	Lowland	0.71	0.20	0.30	1.97
	All Locations	0.901	0.28	0.40	1.56
Sep-18	Upland	0.85	0.48	1.01	1.39
	Lowland	0.89	0.22	0.25	1.97
	All Locations	1.02	0.49	1.09	2.35

Table S4: Soil depth (cm) and soil moisture (%) measured in July and September (2017) and July (2018). Location indicates the alder shrubland patches from which measurements were derived. 'UA', 'WA', and 'DA' denote locations upslope, within, and downslope of alder shrublands, respectively. Black horizontal lines separate sampling campaigns.

Date	***Parameter***	***Location***		***n***	***max***	***min***	***mean***	***std***
Jul-17	Depth (cm)	A1-A5	UA + WA	3	38.3	32.7	35.2	2.9
			DA	5	33	25.5	29.4	3.0
	Moisture (%)		UA + WA	19	67.7	4.3	28.5	23.8
			DA	8	83.9	8.9	55.9	20.9
Sep-17	Depth (cm)	A1/A4	UA + WA	9	66.0	43.6	45.7	21.7
			DA	5	66.7	48.8	56.5	5.4
	Moisture (%)		UA + WA	6	56.1	17.1	28.4	14.2
			DA	-	-	-	-	-
Jul-18	Depth (cm)	A1/A4	UA + WA	12	56	29.2	36.6	7.3
			DA	24	76.2	35.2	53.3	12.1
	Moisture (%)		UA + WA	7	57.6	16.2	36.7	14.9
			Downslope	18	82.7	19.2	51.0	22.6

Table S5: July 23-27, 2018 and September 21-22, 2018. Chemical parameters and constituents (Sample mean and standard deviation). Sample IDs starting with P indicate Pits dug along the A1 transect. Concentrations without a reported standard deviation are single values.

	July 23-27, 2018							
Sample ID	***NO_3-N (mg L^-)***	***NO_3-N std***	***Mn (mg L^-)***	***Mn std***	***Fe^{2+} (mg L^-)***	***Fe^{+2}std***	***SO_4^{2-} (mg L^-)***	***SO_4^{2-} std***

A1_WI_Up	6.52	1.24	0.01	0.00	0.70	0.17	0.44	0.19
A1_WI_Mid	0.51	0.42	0.01	0.00	0.26	0.11	0.51	0.31
A1_WI_Down	0.82	0.98	0.01	0.00	0.22	0.06	0.27	0.12
A1_DS_Seep	0.65	0.11	0.00	0.00	<0.01	<0.01	1.27	0.04
A1_DS_0	4.57	0.35	0.02	0.02	0.47	0.02	0.33	0.13
A1_DS_10	0.02	0.01	0.00	0.00	0.58	<0.01	0.39	0.25
A1_DS_20	0.43	0.10	0.01	0.00	0.31	0.06	1.77	0.22
A1_DS_30	0.03	0.02	0.00	0.00	0.69	0.06	0.65	0.25
A1_DS_40	0.07	0.04	0.00	0.00	0.77	0.01	0.42	0.24
A1_DS_50	0.02	0.01	0.01	0.00	0.67	<0.01	0.39	0.26
A4_WI_Up	5.73	-	0.02	-	0.46	-	1.83	-
A4_WI_Mid	0.70	0.48	0.01	0.00	0.32	0.03	0.53	0.43
A4_WI_Down	2.50	0.45	0.01	0.00	0.2	0.17	0.59	0.49
A4_DS_0	2.08	0.96	0.00	0.00	0.03	0.02	4.50	0.40
A4_DS_10	0.04	0.06	0.03	0.02	0.73	0.90	0.66	0.20
A4_DS_20	0.03	0.04	0.05	0.01	5.21	3.05	0.52	0.23
A4_DS_30	0.02	0.02	0.32	0.05	1.99	1.96	0.62	0.23
A4_DS_40	0.03	0.03	0.12	0.02	1.00	1.05	1.11	0.61
A4_DS_50	0.03	0.03	0.06	0.09	1.87	-	0.55	0.15
Between A1/A4	0.15	0.09	0.01	0.01	0.36	0.09	0.78	0.35
P1_20	6.52	2.01	0.00	0.00	0.11	-	0.35	0.26
P1_40	7.59	2.03	0.01	0.00	0.53	-	0.31	0.09
P2_20	3.57	0.67	0.01	0.01	0.44	-	1.40	0.21
P2_40	8.01	0.25	0.00	0.00	0.22	-	1.83	0.27
P2_60	8.32	1.64	0.01	0.00	0.15	-	5.23	0.46
P3_20	0.03	0.01	0.00	0.00	0.64	-	0.54	0.22
P3_40	0.03	0.02	0.01	0.00	0.15	-	3.41	0.43

September 21-22, 2018

Sample ID	***NO_3-N (mg L^-)***	***NO_3-N std***	***Mn (mg L^-)***	***Mn std***	***Fe^{2+} (mg L^-)***	***Fe^{+2} std***	***SO_4^{2-} (mg L^-)***	***SO_4^{2-} std***
A1_WI_Up	17.73		0.01		0.57		0.22	
A1_WI_Mid	0.58	0.70	0.01	0.02	0.15	0.05	0.20	0.07
A1_WI_Down	1.45	0.75	0.01	0.00	0.18	0.10	0.15	0.04
A1_DS_Seep	0.74	0.24	0.00	0.00	0.00	0.00	35.51	10.52
A1_DS_0	3.11	0.81	0.00	0.00	0.68	0.13	0.20	0.01
A1_DS_10	0.06	0.06	0.00	0.00	0.60	0.06	0.23	0.10
A1_DS_20	0.10	0.01	0.00	0.00	0.26	0.20	1.71	0.46
A1_DS_30	0.02	0.01	0.00	0.00	0.90	0.28	0.41	0.08
A1_DS_40	0.03	0.01	0.00	0.00	0.64	0.08	0.28	0.10
A1_DS_50	0.02	0.01	0.00	0.00	1.72	0.83	0.19	0.06
A4_WI_Mid	3.21	2.78	0.04		0.11	0.02	0.23	0.04

A4_WI_Down	8.44	3.44	0.01	0.01	0.10	0.03	0.29	0.16
A4_DS_0	3.44	2.70	0.00	0.00	0.05	0.01	5.01	0.33
A4_DS_10	0.05	0.05	0.02	0.01	1.33	0.74	5.65	6.12
A4_DS_20	0.02	0.01	0.04	0.01	4.60	1.39	1.60	1.53
A4_DS_30	0.02	0.00	0.22	0.12	1.92	1.15	0.56	0.41
A4_DS_40	0.04	0.04	0.11	0.03	6.75	4.74	1.56	0.49
A4_DS_50	0.03	0.03	0.23	0.23	13.31	7.19	0.25	0.04
Between A1/A4	0.38	0.08	0.00	0.00	0.21	0.21	0.93	0.39
P1_20	4.87	1.15	0.01	0.00	0.78	0.02	0.82	0.07
P1_40	5.45	0.06	0.00	0.00	0.18	0.03	1.56	0.02
P1_60	0.10	0.07	0.16	0.04	0.16	0.04	2.76	1.04
P2_20	0.04	0.00	0.00	0.00	1.34	0.60	0.53	0.23
P2_40	0.06	0.04	0.02	0.01	3.77	3.29	0.25	0.03
P3_20	29.22	10.74	0.00	0.00	0.29	0.03	0.23	0.03
P3_40	28.03	1.15	0.00		0.08		0.15	

Table S6: A statistical comparison of soil pore water concentrations (from Table S5; nitrate-N, ferrous iron, total iron, manganese, and sulfate, respectively) in upland locations compared to lowland locations along the A1 and A4 transects in 2018 (July and September campaigns combined). P-values < 0.05 are considered significant and indicate that 'upland' concentrations are significantly different from 'lowland' concentrations.

Chemical Parameter	*Transect*	*p - value*	*Upland (n)*	*Lowland (n)*

NO_3-N	A1	**<0.001**	31	58
	A4	**<0.001**	19	36
	Both	**<0.001**	56***	94
Fe^{2+}	A1	0.194	10*	15
	A4	**0.021**	6*	9*
	Both	**<0.004**	18***	24
Fe_{Total}	A1	**0.02**	31	58
	A4	**<0.001**	19	36
	Both	**<0.001**	56***	94
Mn	A1	<0.001**	31	58
	A4	**<0.001**	19	36
	Both	0.165	40***	94
SO_4^{2-}	A1	<0.001**	31	58
	A4	0.772	19	36
	Both	**<0.001**	56***	94

*Low *n* due to limited sampling equipment may result in unreliable p values.
**although significantly different, the average Upland Mn and SO_4^{2-} concentrations are greater than the average Lowland Mn concentration and thus do not indicate oxidizing conditions in the Upland area transitioning to reducing conditions in the Lowland area.
***'Upland' includes soil pore water collected both within and outside (between) alder shrublands.

Table S7: Oxygen isotopic composition from soil pore water. July 2017 through September 2018. Black horizontal lines separate sampling campaigns. P-values indicate significant difference between individual seasons and the total mean (All Seasons). P-values less than 0.05 are significant.

Date	***Isotope (‰)***	***n***	***min***	***max***	***mean***	***std***	***P-value***
17-Jul	$\delta^{18}O$	48	-17.3	-15.6	-16.5	0.4	0.42
17-Sep	$\delta^{18}O$	28	-17.0	-13.6	-15.6	0.8	**<0.001**

18-Jul	$\delta^{18}O$	116	-19.4	-14.4	-16.7	0.9	0.01
18-Sep	$\delta^{18}O$	80	-18.4	-12.3	-16.2	1.0	0.15
All Seasons	$\delta^{18}O$	272	-19.4	-12.3	-16.4	0.9	-

Supplemental Figures

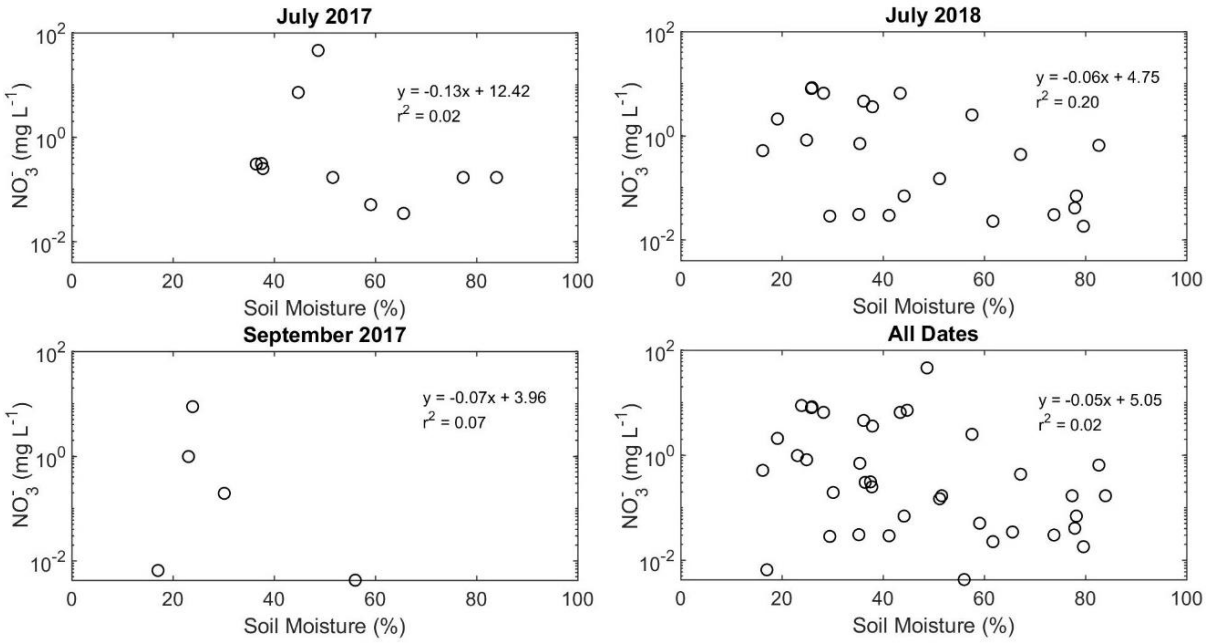

Figure S1: Soil moisture versus NO_3-N from July 2017, July 2018, September 2018, and all three seasons. No direct relationship was observed between soil pore water NO_3-N and soil moisture content. It is worth noting that soil moisture and NO_3-N samples were co-located but collected on different temporal scales to avoid perturbing the rhizon nests during our time-series sampling campaigns.

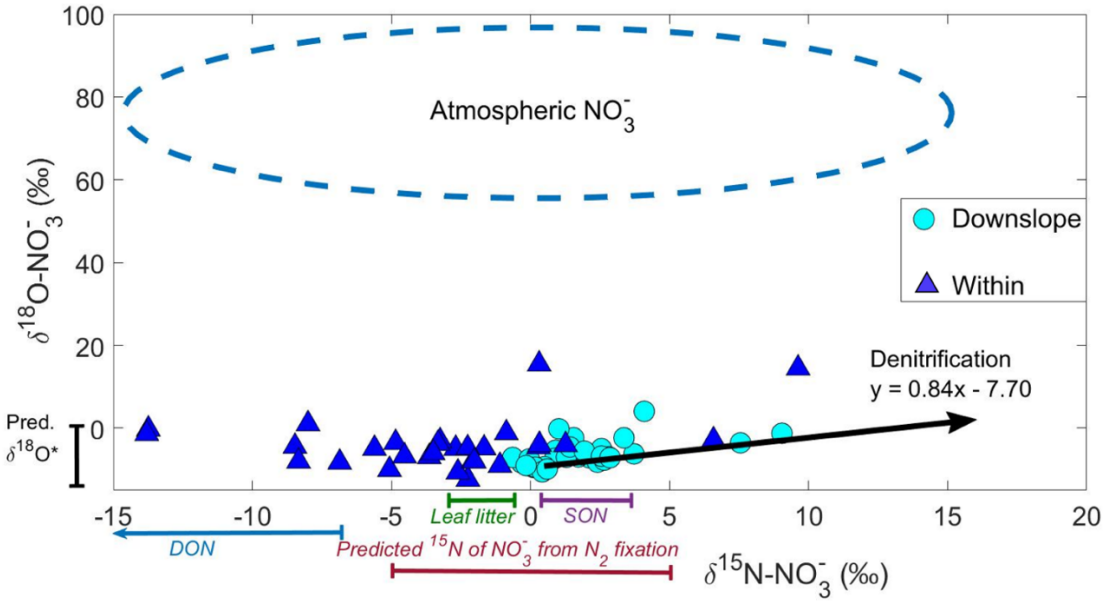

Figure S2: Oxygen ($\delta^{18}O$) versus nitrogen ($\delta^{15}N$) isotopes of soil pore water NO_3^-. Dark blue triangles represent samples within alder shrubland in upland areas. Light blue circles represent samples downslope of alder shrubland in lowland areas. The denitrification process of the downslope samples is denoted by the black arrow inside the plot (y = 0.84x - 7.70). The vertical black line segment (Pred. $\delta^{18}O^*$) denotes the predicted range of $\delta^{18}O$ of NO_3^- produced by microbial nitrification (Eq. 1). The horizontal red line segment indicates the likely $\delta^{15}N$ of NO_3^- range for mineralization and nitrification of organic matter derived from alder material (N-fixation; Kendall and McDonnell, 1998). The likely range of $\delta^{15}N$ of NO_3^- from leaf litter is shown by the horizontal green line segment. The horizontal blue arrow denotes the range of $\delta^{15}N$ of NO_3^- from DON, and the horizontal purple line segment indicates the range of $\delta^{15}N$ of NO_3^- from SON.

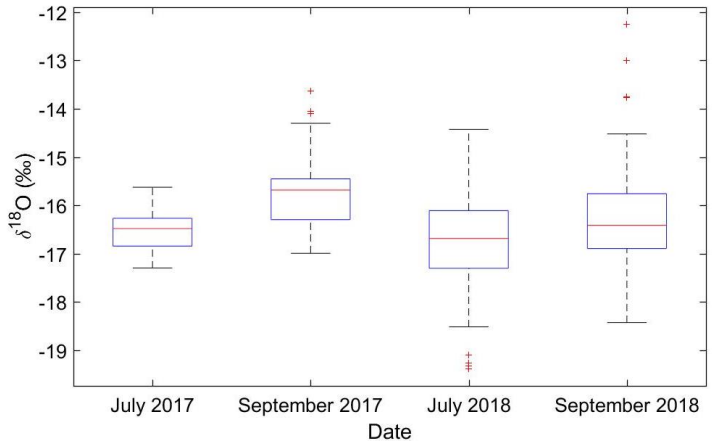

Figure S3: Oxygen isotopes ($\delta^{18}O$) of soil pore water on the KG Hillslope during July and September of 2017 and 2018. The red line within each box represents the sample mean and red crosses indicate outliers. *In September 2017, the mean $\delta^{18}O$ (-15.6 ± 0.8 ‰) was heavier than $\delta^{18}O$ in July 2017, July 2018, and September 2018 ($p < 0.05$) and likely reflects the precipitation event that occurred continuously over the September 2017 sampling campaign.

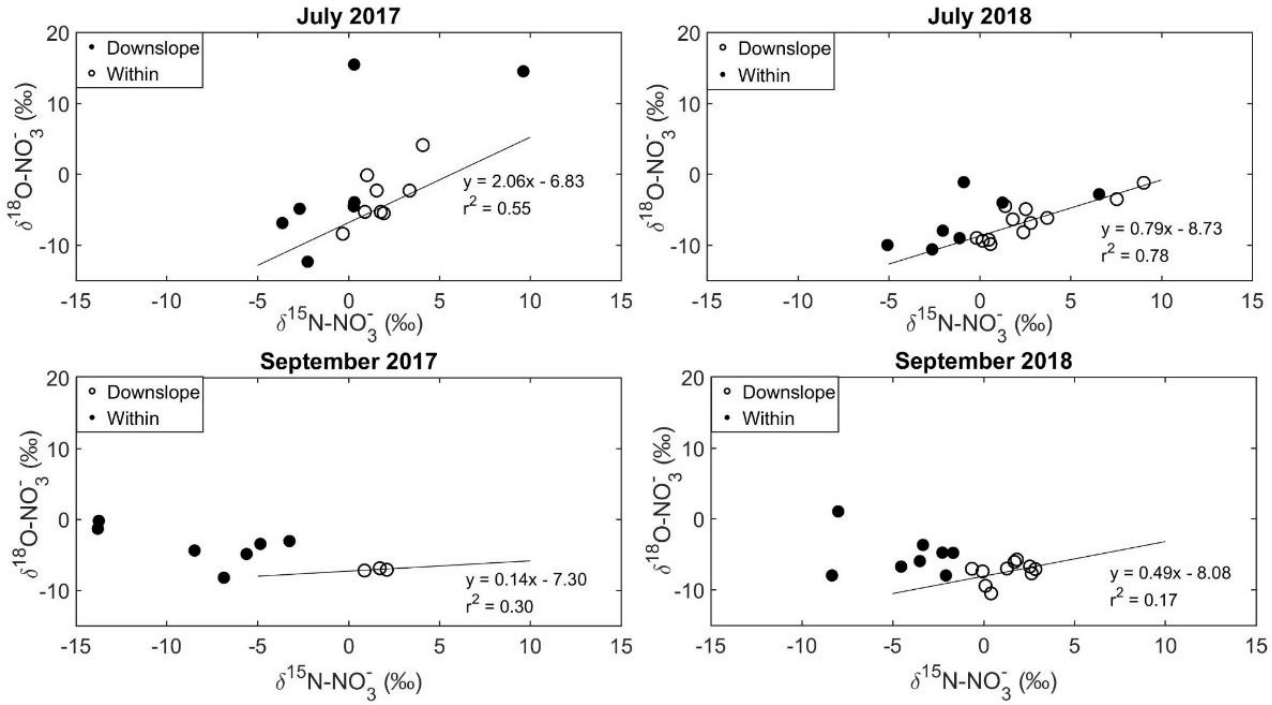

Figure S4: Oxygen ($\delta^{18}O$) versus nitrogen ($\delta^{15}N$) isotopes of soil pore water NO_3^- during July and September (2017 and 2018). Closed black circles represent samples from locations within alder shrubland patches and open black circles represent locations downslope of alder shrubland patches. Black trend lines and equations indicate enrichment of $\delta^{18}O$ and $\delta^{15}N$ of NO_3^- (indicating denitrification) occurring downslope of alder shrublands during each season.

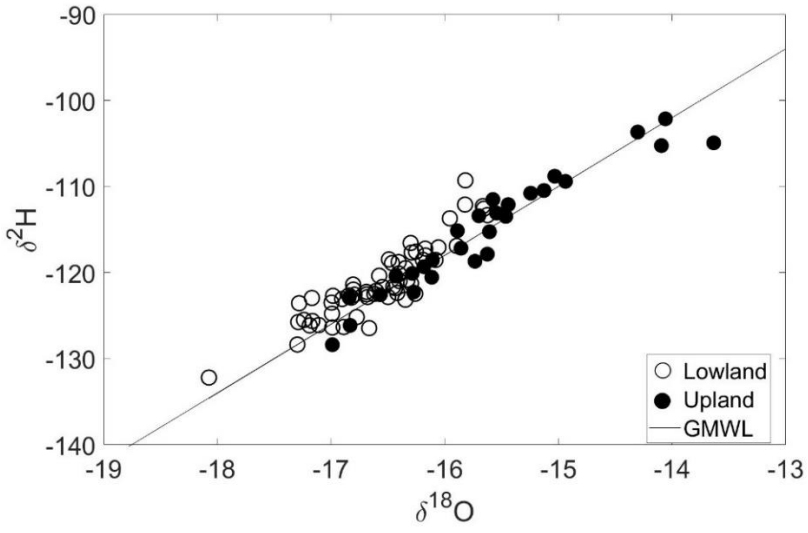

Figure S5: Soil pore water oxygen ($\delta^{18}O$) versus deuterium ($\delta^{2}H$) isotopes during July 2017 and September of 2017 and 2018. $\delta^{18}O$ and $\delta^{2}H$ are plotted against the global meteoric water line (GMWL). Open circles represent lowland locations ($r^2 = 0.81$) and closed circles represent upland locations ($r^2 = 92$).

Supplemental References

Boshers, D. S., Granger, J., Tobias, C. R., Böhlke, J. K., and Smith, R. L.: Constraining the oxygen isotopic composition of nitrate produced by nitrification, Environ. Sci. and Technol., 53, 1206–1216, https://doi.org/10.1021/acs.est.8b03386, 2019.

Böttcher, J., Strebel, O., Voerkelius, S., and Schmidt, H. L.: Using isotope fractionation of nitrate-nitrogen and nitrate-oxygen for evaluation of microbial denitrification in a sandy aquifer, J. Hydrol., 114, 413–424, https://doi.org/10.1016/0022-1694(90)90068-9, 1990.

Brown, C. E.: Coefficient of Variation, in: Applied multivariate statistics in geohydrology and related sciences, edited by: Brown, C. E., Springer, Berlin, Heidelberg, Germany, 155–157, https://doi.org/10.1007/978-3-642-80328-4_13, 1998.

Casciotti, K. L., Sigman, D. M., Hastings, M. G., Böhlke, J. K., and Hilkert, A.: Measurement of the oxygen isotopic composition of nitrate in seawater and freshwater using the denitrifier method, Analytical Chemistry, 74, 4905–4912, https://doi.org/10.1021/ac020113w, 2002.

Craig, H.: Isotopic Variations in Meteoric Waters, Science, 133, 1702-1703, http://doi:10.1126/science.133.3465.1702, 1961.

Granger, J., and Wankel, S. D.: Isotopic overprinting of nitrification on denitrification as a ubiquitous and unifying feature of environmental nitrogen cycling, PNAS, 113, 42, E6391-E6400, https://doi:10.1073/pnas.1601383113, 2016.

Hagedorn, F., and Schleppi, P.: Determination of total dissolved nitrogen by persulfate oxidation, J. Plant. Nutr. Soil Sci., 161, 81-82, https:// doi.org/10.1002/(SICI)1522-2624(200002)163:1<81::AID-JPLN81>3.0.CO;2-1, 2000.

Heikoop, J. M., Throckmorton, H. M., Newman, B. D., Perkins, G. B., Iversen, C. M., Chowdhury, T. R., Romanovsky, V., Graham, D. E., Norby, R. J., Wilson, C. J., and Wullschleger, S. D.: Isotopic identification of soil and permafrost nitrate sources in an Arctic tundra ecosystem, J. Geophys. Res. Biogeosci., 120, 1000– 1017, https://doi:10.1002/2014JG002883, 2015.

Kendall, C., and McDonnell, J. J. (Eds.): Isotope tracers in catchment hydrology, Elsevier Science B.V., Amsterdam, 519-576, https://doi.org/10.1016/C2009-0-10239-8, 1998.

Salmon, V. G., Iversen, C. M., Breen, A. L., Vander Stel, H., and Childs, J.: NGEE Arctic Plant Traits: Plant Biomass and Traits, Kougarok Road Mile Marker 64, Seward Peninsula, Alaska, beginning 2016, Next Generation Ecosystem Experiments Arctic [data set], https://doi.org/10.5440/1346199, 2019.

Schimel, J., and Bennett, J.: Nitrogen mineralization: Challenges of a changing paradigm. Ecology, 85, 591-602, https://doi.org/10.1890/03-8002, 2004.

Sigman, D. M., Casciotti, K. L., Andreani, M., Barford, C., Galanter, M., and Böhlke, J. K.: A bacterial method for the nitrogen isotopic analysis of nitrate in seawater and freshwater, Analytical Chemistry, 73, 4145–4153, https://doi.org/10.1021/ac010088e, 2001.

Throckmorton, H. M., Heikoop, J. M., Newman, B. D., Altmann, G. L., Conrad, M. S., Muss, J. D., Perkins, G. B., Smith, L. J., Torn, M. S., Wullschleger, S. D., and Wilson, C. J.: Pathways and transformations of dissolved methane and dissolved inorganic carbon in Arctic tundra watersheds: Evidence from analysis of stable isotopes, Global Biogeochem. Cycles, 29, 1893–1910, https://doi:10.1002/2014GB005044, 2015.